



## Research Article

<https://doi.org/10.1631/jzus.A2500474>

# Performance analysis and optimization of staggered fin heat exchangers under varying altitudes using machine learning

Kai ZHAO<sup>1,2</sup>, Chunming SHAO<sup>1</sup>, Xiaoxia SUN<sup>1</sup>✉, Yuanqing XIA<sup>2</sup>, Qiangqiang LI<sup>1</sup>, Lili SHEN<sup>1</sup>, Min LIN<sup>1</sup>, Zhi LI<sup>3</sup>

<sup>1</sup>Department of Propulsion System Technologies, China North Vehicle Research Institute, Beijing 100072, China

<sup>2</sup>State Key Lab of Intelligent Control & Decision of Complex Systems, Beijing Institute of Technology, Beijing 100081, China

<sup>3</sup>Power Machinery & Vehicular Engineering Institute, Zhejiang University, Hangzhou 310027, China

**Abstract:** In this study we conduct a comprehensive investigation into the flow and heat transfer behaviors of staggered fin heat dissipation channels across varying altitudes (0-5000 m). The results reveal that higher altitudes lead to a notable deterioration in heat exchanger performance. Specifically, compared to sea-level conditions, elevating the altitude to 5000 m results in a concurrent reduction of 23% in pressure drop and 18% in heat transfer coefficient. Therefore, while existing fin structures meet low-altitude requirements, they require optimization to adapt to high-altitude environments. However, this optimization process involves evaluating a vast number of design schemes. Traditional computational fluid dynamics (CFD) simulations are often too computationally expensive for this task, creating a significant bottleneck. To address this challenge, we established an efficient optimization framework that integrates numerical simulations, machine learning, and an improved Non-dominated Sorting Genetic Algorithm II (NSGA-II). Three machine learning models were evaluated, among which the Gradient Boosting Decision Tree (GBDT) achieved superior predictive accuracy ( $R^2 \approx 1.0$ ) for both heat transfer coefficient and pressure drop. Subsequently, multi-objective optimization was realized utilizing GBDT as a surrogate model coupled with the improved NSGA-II. We find that when the pressure drop is comparable to that of the original structure, the heat transfer coefficient increases by approximately 23% across all tested altitudes. Conversely, when the heat transfer coefficient remains on par with the original design, the pressure drop decreases by about 17%. These findings may help guide the optimal design of next-generation staggered fin heat exchangers suitable for high altitudes.

**Key words:** Staggered fins; High altitude; Machine learning; NSGA-II algorithm

## 1 Introduction

With the widespread application and expanding operational scope of specialized vehicles, environmental adaptability requirements for their power systems have become increasingly stringent (Sun et al., 2024; Xu et al., 2022; Huang et al., 2025). Under diverse and dynamic operating conditions, the cooling system must adapt to drastic fluctuations in

external parameters such as temperature, pressure, and humidity, so as to ensure reliable operation of engines and other critical components (Elsayed et al., 2020; Yang et al., 2024; Ramakrishnan et al., 2022). However, as a critical component of the cooling system, the heat exchanger exhibits high sensitivity to environmental variations, and altitude stands out as an obvious influencing factor (Liu and Liu, 2022; Zhao et al., 2026). At high altitudes, thinner air leads to substantial reductions in atmospheric pressure and air density, and this decline in cooling capacity directly impairs a heat exchanger's heat transfer efficiency (Lang et al., 2024; Li et al., 2025). Consequently, detailed research on altitude-induced performance attenuation is essential for enhancing the adaptability of armored vehicles in complex operating

✉ Xiaoxia SUN, sunxiaoxia616@126.com

Received Sept. 25, 2025; Revision accepted Mar. 13, 2026;  
Crosschecked

© Zhejiang University Press 2026

environments.

In recent years, heat exchanger performance in high-altitude environments has become a popular research topic. For instance, Yang et al. (2024) proved that high-altitude environments lead to a simultaneous decrease in the air-side convective heat transfer coefficient and cooling fan head, substantially degrading overall radiator performance. Moreover, Liu et al. (2020) quantitatively analyzed heat exchangers under different altitude conditions using three-dimensional CFD simulations, further proposing empirical formulas to characterize the attenuation of the heat transfer coefficient induced by high altitude. Notably, atmospheric pressure decreases significantly as altitude rises, so previous studies on heat exchangers operating in low-pressure conditions also hold reference value (Chen et al., 2024). At the same time, Li et al. (2022) found that when ambient pressure decreases, both the heat transfer efficiency and entropy production performance of a heat exchanger decline significantly. Additionally, the adaptability of different heat exchanger fin types under high altitude conditions has been systematically compared: Cai et al. (2017) showed that heat exchangers with louvered fins exhibit the strongest heat dissipation capacity at high altitudes, while those with staggered fins demonstrate better environmental adaptability.

The staggered fin geometry investigated in this study is widely employed in compact heat exchangers for applications where space efficiency and thermal performance are critical. These applications include vehicle radiators, intercoolers for turbocharged engines, oil coolers, and environmental control systems in aerospace and armored vehicles. Such scenarios demand reliable thermal management across diverse operating altitudes, making altitude-adaptive design of staggered fins vital for enhancing equipment durability and performance in plateau regions. To fulfill these rigorous thermal demands, careful design of fin geometric parameters is essential. For reference, studies have highlighted that variations in key structural factors – such as fin length and inclination – can significantly alter convective heat transfer characteristics (Ben-Nakhi and Chamkha, 2006); as such, these results can provide crucial theoretical guidance for optimizing compact heat exchangers.

Previous studies have primarily investigated the macroscopic performance trends of heat exchangers at altitude. Nevertheless, two critical gaps persist. First, the microscale flow and heat exchange mechanisms under high-altitude conditions remain poorly understood. Second, traditional high-fidelity CFD simulations are computationally prohibitive for this task, which makes it difficult to accumulate sufficient data for structural optimization.

Driven by the need for more efficient prediction methods, machine learning has recently emerged as a pivotal research direction. This technology has demonstrated remarkable advantages across multiple heat transfer applications. For instance, Wen et al. (2024) addressed the challenge of predicting heat transfer in supercritical carbon dioxide within the pseudocritical region. Using 11,032 sets of publicly available experimental data, they developed a predictive model with input parameters including mass flow rate, wall heat flux, pressure, and pipe diameter, while setting wall temperature as the output target. By comparing the performance of four algorithms – random forest (RF), GBDT, support vector machine (SVR), and artificial neural network (ANN) – they demonstrated that the ANN could accurately capture the heat transfer deterioration phenomenon when the fluid temperature approaches or exceeds the pseudocritical value. Beyond single-phase flow applications, machine learning has also demonstrated transformative potential in more complex heat transfer scenarios, such as those involving phase change phenomena like boiling and condensation. Recent studies have successfully deployed advanced neural networks and ensemble learning algorithms to predict boiling heat transfer coefficients and critical heat flux, effectively capturing the non-linear nature of bubble dynamics and liquid-vapor interfacial behaviors (Mustafa and Kandlikar, 2025).

Meanwhile, the design of advanced heat exchangers incorporating phase change materials (PCMs) is another promising domain. For example, detailed numerical investigations have demonstrated the efficacy of multi-layer PCMs in enhancing heat transfer under periodic boundary conditions (Sadeghi et al., 2020). To further optimize PCM-based systems and efficiently explore their vast design spaces, researchers are increasingly deploying machine

learning techniques. In one study, Shahsavari et al. (2022) used 3D numerical simulations to investigate the influence of tip clearance (TC) between annular fins on heat transfer characteristics in battery thermal management systems (TMS) containing phase change materials (PCM). They found that a TC of 0.5 mm maximizes the heat transfer rate while minimizing PCM melting time. Furthermore, they developed an integrated machine learning model based on GBDT, enabling the prediction of liquid fraction, temperature distribution, and thermal entropy generation rate with high precision. In a related context, the application of multi-layer PCMs in tubular heat exchangers subjected to periodic boundary conditions has also proven effective in enhancing thermal performance.

Although applications of machine learning in the field of heat transfer are becoming increasingly mature, recent work has explored coupling machine learning with multi-objective optimization to address the challenges of numerous parameters and conflicting objectives. As an example, Li et al. (2020) evaluated the performance of staggered fins under low-temperature conditions based on fluid structure coupling theory, and obtained the Pareto front using a genetic algorithm; their results showed that the Jugensson-Fischer factor increased by 4.4% to 9.6% while the peak stress decreased by 21% to 42%. Also, He et al. (2024) combined an ANN and NSGA-II to perform multi-objective optimization of the fin geometry of a plate fin heat exchanger, resulting in a 23% reduction in the hot end's average temperature. Moreover, Tikadar and Kumar (2024) proposed a multi-parameter framework with an ANN to optimize the layout of laminar flow heat dissipation fins; this framework improved the overall performance by 19% to 35% while keeping the pump power essentially constant. Collectively, these studies indicate that integrating machine learning with multi-objective optimization can not only effectively resolve the complexities of multiple parameters and conflicting objectives in heat transfer system design, but also shorten the optimization cycle.

This study elucidates the mechanism by which altitude affects the microscale heat transfer performance of staggered fins, addressing the insufficient understanding of microscale flow and heat transfer mechanisms under high-altitude conditions. Specifically, a systematic comparison is

conducted among three machine learning models—ANN, DT, and GBDT—to evaluate their performance in establishing the mapping relationships among key fin geometric parameters, altitude parameters, and two critical metrics: pressure drop and heat transfer coefficient. Finally, based on the trained machine learning surrogate model, an improved NSGA-II algorithm incorporating an adaptive crossover and mutation rate strategy is proposed for multi-objective optimization. This algorithm overcomes the inherent limitations of the standard NSGA-II, and together with the surrogate model, effectively addresses the issue of inefficient optimization due to computationally expensive CFD simulations. This optimized strategy synergistically enhances the flow and heat transfer characteristics of staggered fins under high-altitude conditions; accordingly, it improves the overall performance of the heat exchanger and offers a novel approach for high-altitude adaptive design of thermal engineering equipment.

## 2 Materials and methods

In this study, a synergistic framework integrating numerical simulations, machine learning, and multi-objective optimization is established to address the thermal-fluid performance degradation of staggered fins in high-altitude environment and accordingly improve performance. The overall workflow of this framework is illustrated in Fig. 1. Specifically, as shown in the first stage of Fig. 1, a CFD model for periodic staggered fin units was developed, with the RNG  $k-\varepsilon$  turbulence equation adopted to simulate the flow and heat transfer characteristics at altitudes ranging from 0 to 5000 m. Boundary layer mesh generation and experimental validation were performed to ensure the reliability of the CFD model, enabling quantitative determination of the influence laws of altitude on pressure drop, heat transfer coefficient, and boundary layer thickness. Then, corresponding to the second stage in Fig. 1, a dataset was generated based on parametric geometry, and the predictive performances of three machine learning models (DT, ANN, and GBDT) were compared. The optimal model achieved millisecond-level prediction time for pressure drop and heat transfer coefficient, thus replacing

time-consuming CFD simulations. Finally, in line with the third stage of Fig. 1, the well-performing machine learning model was coupled with the improved NSGA-II to synergistically optimize fin length and fin spacing, enhancing the adaptability of the staggered fins to high-altitude environments.

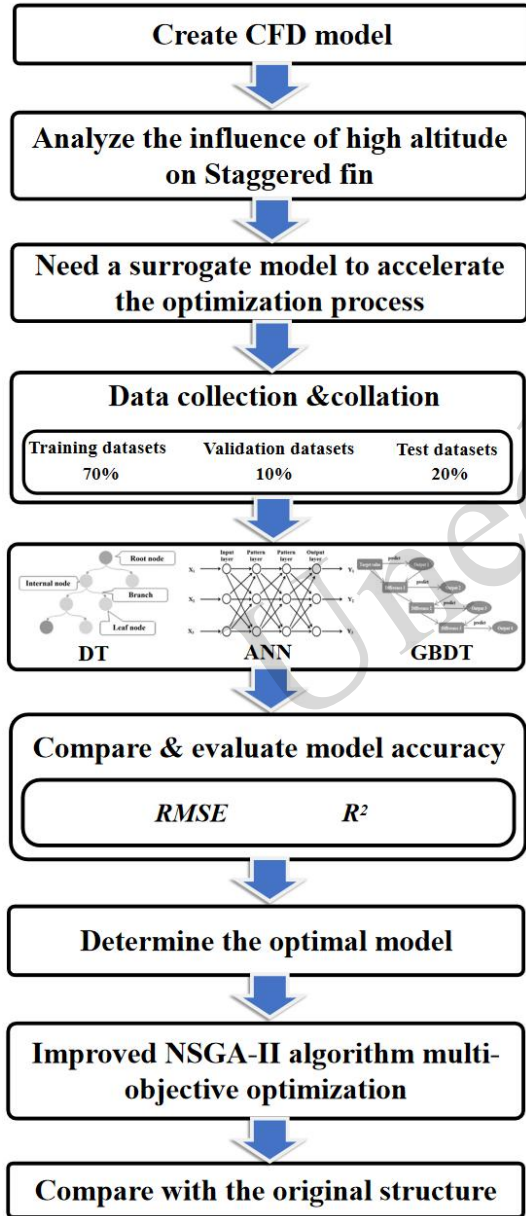


Fig. 1 Flowchart of the overall methodology

### 2.1 Geometric models

A staggered fin structure from the heat exchanger experiments documented by Kay and

London (1984) was selected for this study; the specific air-side structural dimensions are presented in Table 1. Given the repetitive and stackable characteristics of the heat exchanger structure, a staggered fin unit was established using periodic boundary conditions, as illustrated in Fig. 2 and Fig. 3. The main parameters of this unit are fin length, fin height, fin spacing, and fin thickness.

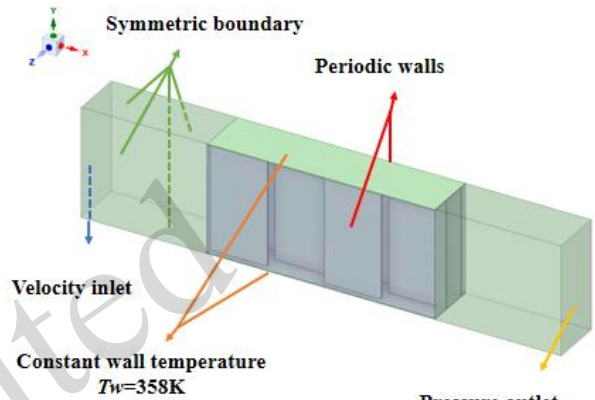
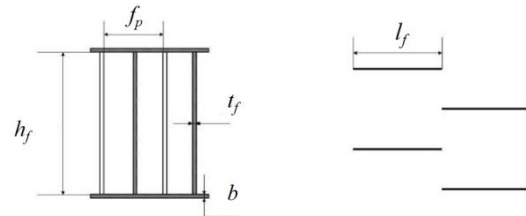


Fig. 2 Computational model of a staggered fin unit with boundary conditions



(a) Front view (b) Top view  
Fig. 3 Schematic diagram of the staggered fin structural parameters

Table 1 Geometric dimensions of the fin

Structural parameter	Fin length ( $l_f$ )	Fin height ( $h_f$ )	Fin spacing ( $f_p$ )	Fin thickness ( $t_f$ )
Value (mm)	4.52	8.75	2.083	0.102

### 2.2 Simulation setup

In this work we focus on the air-side heat transfer process of the heat exchanger, where the solid component is aluminum (fins), the working fluid is air (treated as incompressible with constant physical properties), and the upper and lower walls are configured as constant temperature walls (350 K) to

simulate the heat source provided by the water side (coolant) during operation; the left and right boundaries are defined as periodic boundary walls, the inlet is set as a velocity inlet condition, and the outlet as a pressure outlet boundary condition. For the numerical solutions, the *SIMPLEC* algorithm is employed, with second order upwind schemes applied to the energy and momentum equations, and the convergence criteria for the continuity, momentum, and energy equations are set to  $10^{-6}$ .

The following assumptions are adopted in the numerical simulations: (1) Air is treated as incompressible with constant thermophysical properties at each altitude (although properties vary across altitudes as given in Table 2); (2) The fin material (aluminum) is homogeneous and isotropic with constant thermal conductivity; (3) The upper and lower walls are maintained at a constant temperature of 350 K, and the inlet airflow is uniform and steady; (4) Radiative heat transfer is neglected since forced convection dominates; (5) The fin surfaces are assumed to be perfectly clean with no fouling; (6) The flow and temperature fields are assumed to be periodically fully developed, allowing a single staggered fin unit with periodic boundaries to represent the entire heat exchanger core.

Under laminar flow conditions, the governing equations established in this study consist of the continuity equation, energy equation, and momentum equation. The detailed mathematical model is presented in Section S1 of the Electronic Supplementary Materials (ESM).

In this study we use an altitude range of 0–5000 m, with six representative operating conditions selected: 0 m, 1000 m, 2000 m, 3000 m, 4000 m, and 5000 m (detailed parameters are provided in Table S1 in the ESM). Across these conditions, air pressure and density exhibit significant variations. Regarding air viscosity, according to the kinetic theory of gases and Sutherland's law, the dynamic viscosity of a gas is primarily a function of temperature and is largely independent of pressure within a moderate pressure range (Miao et al., 2025). Since the inlet air temperature is maintained at a constant 288.15 K in this work, the variation in viscosity caused by altitude-induced pressure changes is negligible. Therefore, the air viscosity is treated as a constant value ( $1.89\text{E-}05$  Pa·s) in the simulations. Moreover,

the inlet temperature is maintained at a constant 288.15 K.

### 2.3 Mesh generation and model validation

As shown in Fig. S1 (in the ESM), the mesh generation was conducted using *ANSYS ICEM CFD* software, with boundary layers defined at the fluid-solid coupling interfaces. To confirm the model's accuracy, the  $j$  and  $f$  factors obtained from simulations were compared with experimental data reported by Kay and London (1984). These two dimensionless parameters are used to assess heat transfer performance and frictional loss in heat dissipation systems, respectively; their specific expressions are:

$$j = \frac{D_H}{4L} Pr^{2/3} \ln\left(\frac{T_w - T_{in}}{T_w - T_{out}}\right) \quad (1)$$

$$f = \frac{\Delta p D_H}{2\rho u^2 L} \quad (2)$$

where  $D_H$  is the hydraulic diameter,  $L$  is the channel length, and  $T_w$ ,  $T_{in}$ , and  $T_{out}$  are the wall temperature, air inlet temperature, and air outlet temperature, respectively.  $\Delta p$  represents the pressure difference between the inlet and outlet. A comparison between the simulated and experimental  $j$  and  $f$  factors is shown in Fig. 4. To quantify the reliability of the numerical results and address potential uncertainties, the error was systematically analyzed. The average deviations were found to be 8% for the  $j$  factor and 3% for the  $f$  factor, both of which are within the acceptable engineering threshold of 10%. These minor discrepancies are primarily attributed to the idealized periodic boundary conditions and the inherent simplifications of the turbulence model. Consequently, the CFD model exhibits sufficient accuracy and low uncertainty in predicting the thermal-hydraulic performance of staggered fins across varying altitudes.

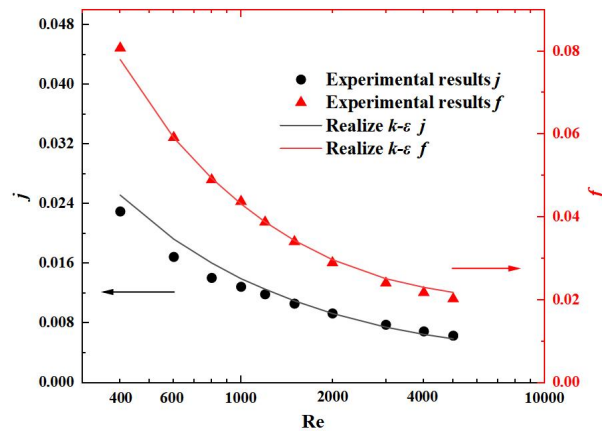


Fig. 4 Validation of the simulations in comparison to experimental data

## 2.4 Machine learning modeling

To address the inefficiencies of traditional CFD simulations in supporting multi-objective optimization for staggered fin heat exchangers, a machine learning surrogate model was introduced. Notably, in this study the operating conditions required for model training were generated through CFD simulations; these simulations, while reliable for capturing the thermal-fluid characteristics of staggered fins under different altitude and geometric parameter combinations, still impose a non-negligible computational burden. High-resolution boundary layer meshing and the iterative convergence of turbulence equations mean that each CFD run for a single set of fin geometric parameters and altitude conditions consumes substantial computational resources, making repeated large-scale simulations impractical.

Relying solely on CFD becomes a significant issue in subsequent multi-objective optimization: this process typically requires evaluating thousands of candidate solutions. If each evaluation were to depend directly on CFD simulations, the total computation burden would become prohibitive, severely prolonging the optimization cycle and hindering efficient screening of fin designs. In contrast, once it is trained on the pre-generated CFD dataset, the machine learning surrogate model can rapidly predict key performance indicators (pressure drop and heat transfer coefficient) for any new candidate design. This approach not only retains the accuracy derived

from CFD, but also eliminates the need for repeated time-consuming CFD simulations during the optimization process; accordingly, this can accelerate exploration for solutions and enhance screening efficiency.

To systematically evaluate the potential of data-driven methods in predicting fin performance, we selected three representative modeling approaches—Decision Tree (DT), Artificial Neural Network (ANN), and Gradient Boosting Decision Tree (GBDT). These models represent distinct algorithmic paradigms, ranging from rule-based and connectionist models to ensemble learning strategies. The fundamental principles and characteristic strengths of these three methodologies are illustrated in Fig. S2 (ESM). By cross-validating their predictive accuracies, we offer an objective basis for selecting the optimal surrogate model for the ensuing optimization tasks.

The screening of proxy models aims to provide reliable tools for parameter optimization, and therefore it is first necessary to clarify the core optimization variables of staggered fin heat exchangers. Among the key structural parameters of staggered fins—such as fin thickness, fin spacing, fin height, and fin length—we identify fin length and fin spacing as the core optimization variables. Fin length and fin spacing are adjustable in practice and are also closely correlated with the heat sink's thermal-hydraulic behavior: changes in fin length directly affect the heat transfer area and flow disturbance intensity, while variations in fin spacing impact airflow resistance and boundary layer development. Thus, both parameters are critical for alleviating altitude-induced performance degradation. For the parametric design of these two core variables and altitude conditions, we set the adjustment ranges and intervals as follows: the fin length is adjusted in five equal intervals within the range of 2 mm to 10 mm, the fin spacing is divided into six intervals from 1.5 mm to 2.5 mm, and the altitude covers six representative intervals ranging from 0 m to 5000 m. By combining these three parameter dimensions, a total of  $(5 \times 6 \times 6 = 180)$  operating conditions are generated to support the training of the three machine learning models. This dataset is further divided into three subsets following standard test-train splitting: 70% is used as the input for model training, 10% is

allocated as the validation set, and the remaining 20% is reserved as the testing set to evaluate model performance.

All input and output variables undergo Z-score standardization (with the mean  $\mu$  and standard deviation  $\sigma$  calculated exclusively from the training set to prevent data leakage), while the validation set has the identical scaling parameters applied. The standardization formula is as follows:

$$Z = \frac{x - \mu}{\sigma} \quad (3)$$

where  $Z$  represents the standardized variable,  $\mu$  represents the mean of  $x$  in the training dataset, and  $\sigma$  is the standard deviation of  $x$  in the training dataset.

The results are then compared to determine which model is most effective in forecasting the thermal transfer efficiency of staggered fins under diverse fin parameters. We evaluate the predictive performance of the two models using  $R^2$  and  $RMSE$ , and also compare their precision and generalization abilities (Xie and Wang, 2025).

$R^2$ , also known as the coefficient of determination, is defined as follows:

$$R^2 = 1 - \frac{\sum_{i=1}^n (y_i - \hat{y}_i)^2}{\sum_{i=1}^n (y_i - \bar{y})^2} \quad (4)$$

In analyzing variables, the coefficient of determination is a value between 0 and 1 that indicates the goodness of model fit. It is determined based on the initial values of  $n$  data points (denoted as  $y_i$ ), the mean value of  $y$ , and the predicted values (denoted as  $\hat{y}_i$ ). As the coefficient of determination approaches 1, the model fit improves.

$RMSE$  (root-mean-square error) is a measure of the degree of deviation between the predicted values and the true values.

$$RMSE = \sqrt{\frac{1}{n} \sum_{i=1}^n (y_i - \hat{y}_i)^2} \quad (5)$$

In the given formula,  $n$  represents the number of data points,  $y_i$  represents the actual values, and  $\hat{y}_i$  represents the predicted values. As the  $RMSE$  value approaches zero, this indicates a more accurate prediction result.

## 2.5 Multi-objective optimization method based on improved NSGA-II

For multi-objective optimization, we introduce an improved NSGA-II to drive the global optimization process, aiming to enhance the thermal-fluid performance of staggered fin heat exchangers in high-altitude environments. As a second-generation non-dominated sorting genetic algorithm, the standard NSGA-II retains the global optimization capability of its predecessor while significantly reducing computational complexity through a rapid non-dominated sorting strategy. However, to balance global exploration and local refinement during the fin structure optimization, we improve upon the algorithm, focusing specifically on enhancements to crossover and mutation operators. A dynamic adaptive strategy is designed to adjust the crossover and mutation rates: this strategy modulates the two key hyperparameters with the iterative process, strengthening the algorithm's ability to explore new solution spaces in early stages and refine optimal solutions in later stages; this ultimately accelerates convergence toward the Pareto front and improves the efficiency and reliability of the optimization results.

The crossover rate and mutation rate are critical hyperparameters that significantly influence the search behavior of the algorithm, affecting the direction of population evolution and the convergence performance. Our proposed adaptive strategy aims to achieve a dynamic balance between global exploration and local exploitation during the evolutionary process. In the early stages of optimization, a higher crossover rate and lower mutation rate are adopted to promote population diversity and global search capability. In the later stages, the crossover rate is gradually reduced in order to preserve well-performing individuals, while the mutation rate is increased to enhance local refinement and the ability to escape local optima. The mathematical expressions corresponding to these concepts are provided as follows:

$$P_c(t) = P_{c0} e^{-\beta_c t / T_{max}} \quad (6)$$

$$P_m(t) = P_{m0} (1 - e^{-\beta_m t / T_{max}}) \quad (7)$$

Here,  $P_c(t)$  denotes the crossover probability;

$P_m(t)$  is the mutation probability;  $t$  is the current iteration number;  $T_{max}$  represents the maximum iteration number;  $P_{c0}$  and  $P_{m0}$  denote the initial crossover probability and initial mutation probability, respectively;  $\beta_c$  and  $\beta_m$  are decay coefficients that control the rate at which the crossover probability and mutation probability change with proceeding iterations, respectively.

### 3 Results

#### 3.1 Staggered fin pressure drop and heat transfer coefficient variations with altitude

To clarify the intrinsic reason for altitude-induced performance changes, we first analyze the variation of Reynolds number (a key flow characteristic parameter) with altitude. As shown in Fig. 5, when the inlet velocity is fixed at  $v = 9.68$  m/s, the Reynolds number decreases from  $\sim 1200$  (0 m) to  $\sim 700$  (5000 m), which is attributed to the significant reduction in air density at high altitudes. This change in Reynolds number further affects the flow and heat transfer performance of the fin channel, as reflected in the variations of pressure drop and heat transfer coefficient.

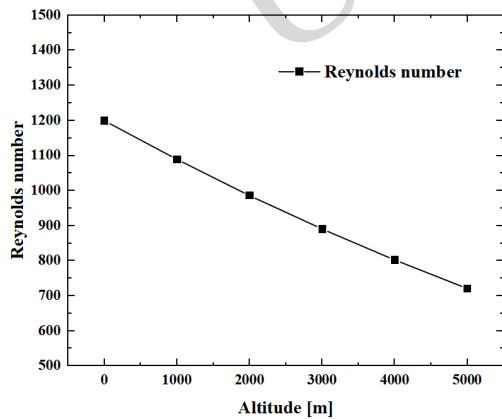


Fig. 5 Variation of Reynolds number with altitude

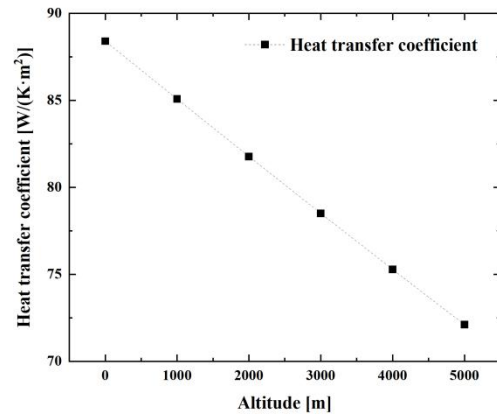


Fig. 6 Pressure drop at different altitudes

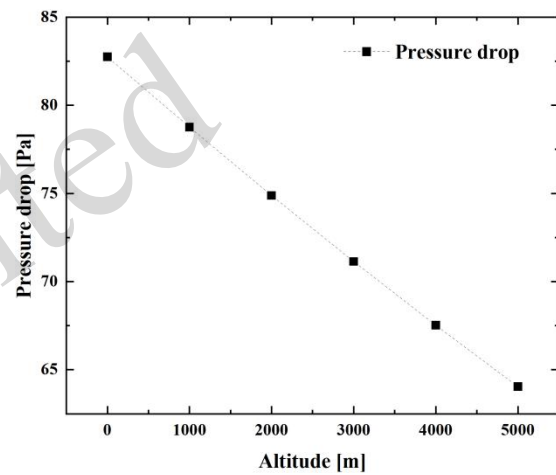


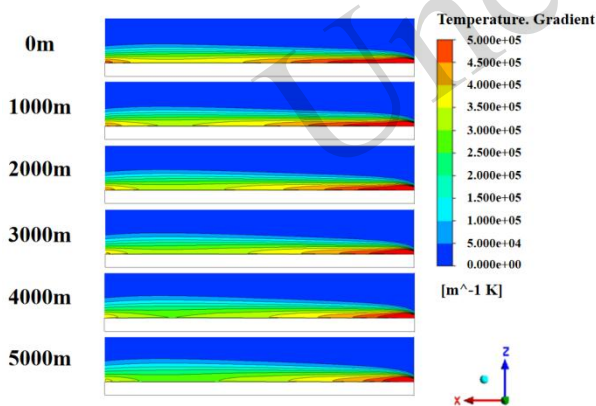
Fig. 7 Heat transfer coefficients at different altitudes

The pressure drop across the heat dissipation channel at varying altitudes is shown in Fig. 6. As the altitude increases, the pressure drop tends to decrease, with the value at 5000 m being 23% lower than at sea level. This reduction occurs because higher altitudes correspond to lower air density, which decreases the mass flow rate at a given velocity. Consequently, fewer air molecules interact with the wall surface to generate friction, leading to reduced loss in pressure. The heat transfer coefficient of the channel is presented in Fig. 7. In keeping with the flow characteristics, the heat transfer coefficient also exhibits a downward trend, decreasing by 18% at 5000 m relative to sea level.

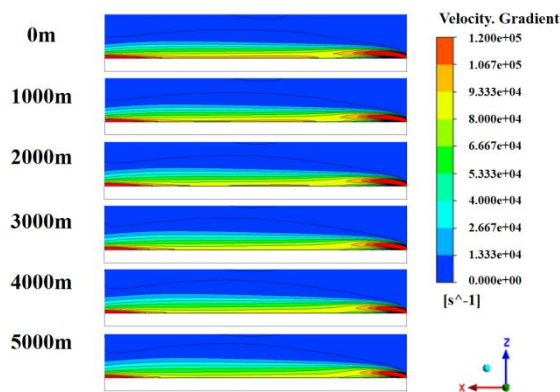
#### 3.2 Theoretical analysis of boundary layers for the staggered fin heat exchanger at varying altitudes

To explain the reasons behind the changes in

heat transfer performance caused by altitude variations, the flow field and temperature field near the fin surface are investigated using boundary layer theory. Fig. 8 illustrates the variations in near-wall temperature and velocity gradients across different altitudes. As the altitude increases, both gradients exhibit noticeable decreases. Furthermore, as the flow and temperature fields develop farther away from the fin surface, the decay rates of these gradients slow down more markedly at higher altitudes; this phenomenon suggests the presence of a thicker boundary layer under such conditions. This boundary layer thickening is inherently driven by the reduction in air density, which dampens near-wall velocity fluctuations and impairs the heat transfer efficiency as a result. Simultaneously, the decrease in Reynolds number promotes stabilization of the laminar flow, further suppressing the outward diffusion of momentum and thermal gradients. Consequently, both the temperature and velocity gradients diminish in magnitude, and their decaying trends become more gradual as the distance from the wall increases.



(a) Temperature gradient



(b) Velocity gradient

**Fig. 8 The distribution of temperature gradient and velocity gradient near the fin surface at different altitudes**

According to the definition of the flow boundary layer, the boundary layer thickness  $\delta$  is the distance from the wall at which the velocity reaches 99% of the mainstream velocity; this corresponds to the flow boundary layer. In this study, the gradient of the velocity in the Z-direction equaling zero is used as the criterion for determining the flow boundary layer, as expressed by:

$$\frac{\partial u}{\partial z} = 0 \quad (8)$$

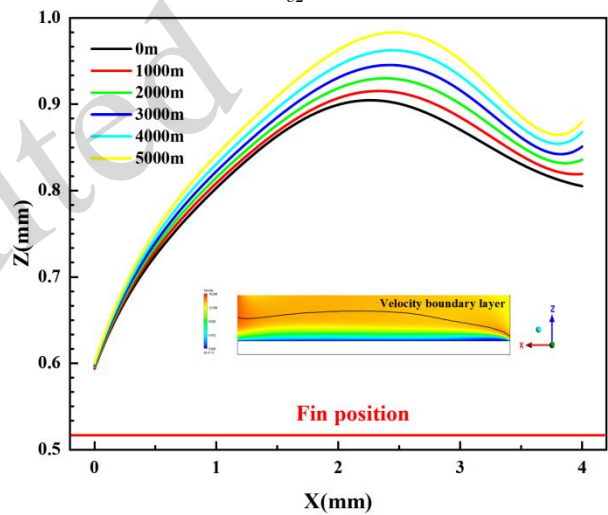


**Fig. 9 Variation of the velocity boundary layer on the fin surface at different altitudes**

As depicted in Fig. 9, the velocity boundary layer thickness on the fin surface increases with increasing altitude. This figure presents the velocity boundary layer profiles at different altitudes (from 0 m to 5000 m), indicating that the boundary layer thickness grows at higher altitudes, particularly near the point of maximum thickness. Specifically, as the altitude increases from 0 m to 5000 m, the boundary layer thickness consistently increases, as evidenced by the peak of the curve shifting to a higher Z-value. This phenomenon can be attributed to the decrease in air density, which enhances fluid momentum diffusion at higher altitudes, thereby increasing the velocity boundary layer thickness.

The thermal boundary layer is generally defined as the region where the excess temperature reaches

99% of the incoming excess temperature, corresponding to the thickness  $\delta_t$  of the thermal boundary layer. In this study, the incoming temperature is 288.15 K and the wall temperature is 350 K. Therefore, the temperature  $T$  at the outer boundary of the thermal boundary layer is:

$$T=0.01 \times (T_W - T_\infty) + T_\infty = 288.77K \quad (9)$$

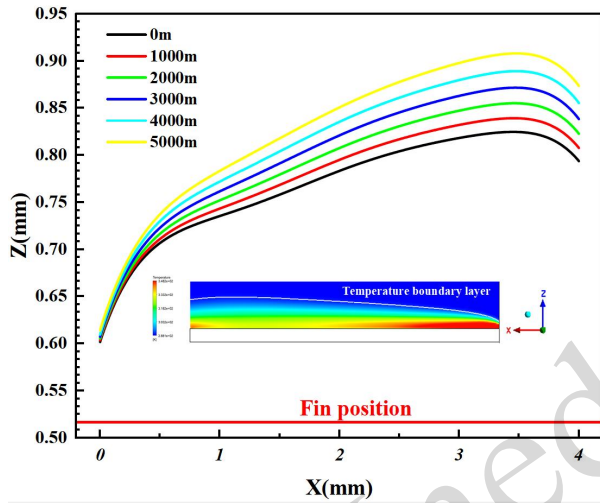


Fig. 10. Variation of the thermal boundary layer on the fin surface at different altitudes

Following this definition, the variation in the thermal boundary layer on the fin surface at different altitudes is presented in Fig. 10. With increasing altitude, the thermal boundary layer gradually expands outward. Like the flow boundary layer, the thermal boundary layer exhibits a thickening trend as the altitude increases from 0 m to 5000 m, with the peak of the curve shifting upward in the  $Z$ -direction. However, the farthest extent of the thermal boundary layer lags behind that of the flow boundary layer. This is primarily due to the reduction in air density, which enhances thermal diffusion. However, the rate of thermal diffusion is relatively slow compared to the rate of momentum diffusion, resulting in the thermal boundary layer extending more slowly than the flow boundary layer.

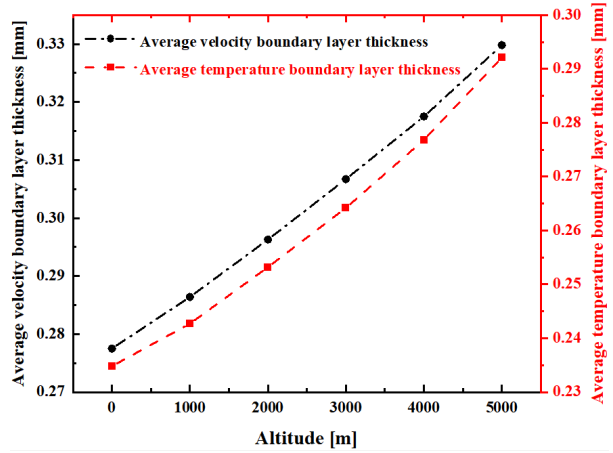


Fig. 11 Variation of average boundary layer thickness on the fin surface with altitude

By applying an integral weighting process to the positions of the near-wall flow boundary layer and the thermal boundary layer, we obtain:

$$\bar{\delta} = \frac{\int_0^{0.00452} \delta dx}{\int_0^{0.00452} x dx} \quad (10)$$

$$\bar{\delta}_t = \frac{\int_0^{0.00452} \delta_t dx}{\int_0^{0.00452} x dx} \quad (11)$$

Here,  $\bar{\delta}$  and  $\bar{\delta}_t$  represent the average flow boundary layer thickness and average thermal boundary layer thickness, respectively. The variation in the average boundary layer thickness on the fin surface at different altitudes is shown in Fig. 11. Compared to sea level, at an altitude of 5000 m, the average velocity boundary layer thickness increases by 19%, while the average thermal boundary layer thickness increases by 24%. The fact that the thermal boundary layer thickness increases more significantly than the velocity boundary layer thickness can be attributed to the greater enhancement of thermal diffusion relative to momentum diffusion.

Now that we have clarified the variation in average boundary layer thickness on the fin surface in response to different altitudes, it is now important to use the wall heat flux to quantify the impact of altitude on heat transfer performance. As previously established, the wall temperature and inlet air temperature are held constant (resulting in an unchanged temperature difference for heat transfer);

under such conditions, the wall heat flux can directly reflect the extent to which altitude impairs the heat transfer capacity of the fins. Fig. 12 illustrates the distribution of wall heat flux along the  $X$ -direction of the fin surface. One can observe that the wall heat flux decreases significantly with increasing altitude; the reduction is especially prominent in the middle region of the fin. This trend is closely related to the decrease in air density and the consequent reduction in heat transfer capability. Furthermore, if the minimum wall heat flux  $q_t=10\text{kW/m}^2$  is used as the threshold to define the weak heat transfer region on the fin surface, it can be found that the effective high-efficiency heat transfer area on the fin surface is considerably reduced at higher altitudes. Such a result indicates that the length of the effective heat transfer region on the fin surface gradually decreases at higher altitudes. The ultimate result is degradation of the overall heat transfer performance.

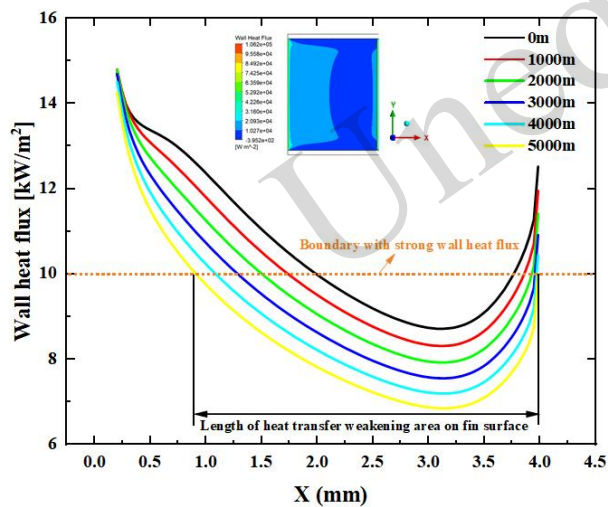


Fig. 12 Distribution of wall heat flux on the fin surface at different altitudes

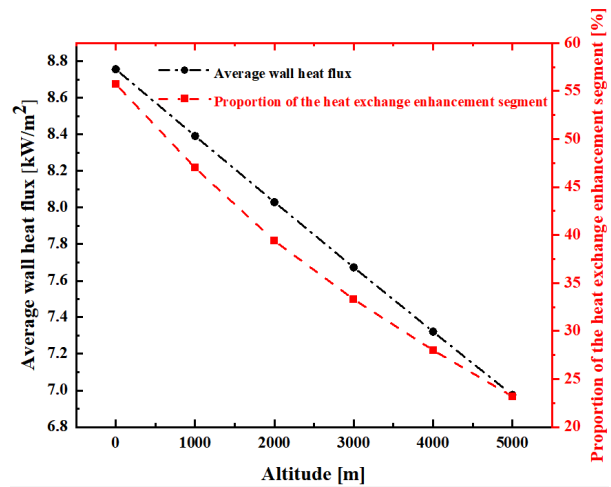


Fig. 13 The effects of different altitudes on the average wall heat flux and the proportion of high-efficiency heat transfer regions on the fin surface

The effects of different altitudes on the average wall heat flux and the proportion of high-efficiency heat transfer regions on the fin surface are showcased in Fig. 13. In comparison to sea level, the average wall heat flux at an altitude of 5000 m decreases by 20%, and the proportion of high-efficiency heat transfer regions relative to the total heat transfer area of the fin decreases by 58%.

### 3.3 Comparison of the machine learning models

From the above analyses, it is evident that the heat transfer performance of staggered fin heat exchangers degrades significantly as altitude increases. While the existing fin structure can meet heat dissipation requirements at low altitudes, its adaptability to high-altitude environments is insufficient—thus there is an urgent need to optimize the fin structure to enhance its thermal-fluid performance at high altitudes.

Notably, the optimization of fin structure requires continuous testing of novel design schemes to verify the improvement effects. However, if traditional CFD is still used to evaluate each new fin structure, the cumulative computational burden will be high. This is because each CFD simulation needs to resolve high-resolution boundary layers and iterate through turbulence equations, making it difficult to efficiently perform the relevant optimization operations. To address this bottleneck and accelerate the optimization process, we sought to develop a fast

and precise surrogate model for predicting fin performance; machine learning (ML), with its ability to map complex thermal-fluid relationships and achieve rapid inference, emerged as the ideal strategy for developing such a model.

To implement this ML-based surrogate model, we leveraged the standardized dataset generated from the CFD simulations (Section 2.7), which covers 180 representative operating conditions of staggered fins under different altitude and geometric parameter combinations. Based on this dataset, three representative ML models—DT, ANN, and GBDT—were trained and validated. The detailed hyperparameter settings for these models, which were obtained via a grid search method to ensure reproducibility, are provided in Table S2 in the ESM. As summarized in Table S3 (ESM), the GBDT model consistently outperformed the others, achieving an  $R^2$  near 1.0 and minimal  $RMSE$  across the training, validation, and testing datasets. The complete set of regression plots, illustrating the predictive performance for both pressure drop and heat transfer coefficient, is presented in Figs. S3-S4 in the ESM. Based on these results, GBDT is selected as the best surrogate model for subsequent multi-objective optimization.

### 3.4 Multi-objective optimization of pressure drop and heat transfer coefficient

Next for the optimization with the GBDT employed as the surrogate model, the optimization variables are fin length (2-10 mm) and fin spacing (1.5-2.5 mm), while all other structural parameters remain unchanged. The final optimization results are presented in Fig. 14, which provides a comparative analysis with the original design parameters (fin spacing: 2.083 mm; fin length: 4.52 mm).

Fig. 14 illustrates that the obtained Pareto front can be categorized into three distinct regions: a low flow resistance region, a comprehensive optimization region, and a high heat transfer coefficient region. In the low flow resistance region, the heat transfer coefficient is generally lower than that of the baseline design, indicating that the solutions in this region achieve lower flow resistance at the expense of thermal performance. These fin structures are characterized by larger fin spacing and shorter fin

length. The increased spacing reduces flow obstruction and pressure drop, while the shorter fin length minimizes flow disturbance – both of these contribute to lower flow resistance.

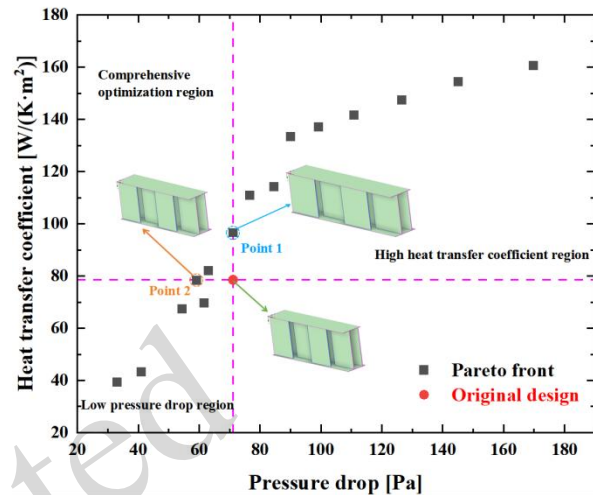
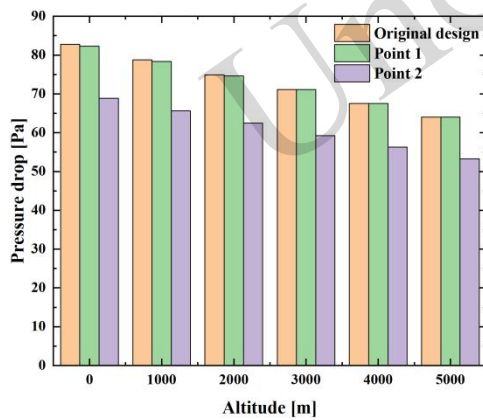


Fig. 14 The multi-objective optimization results

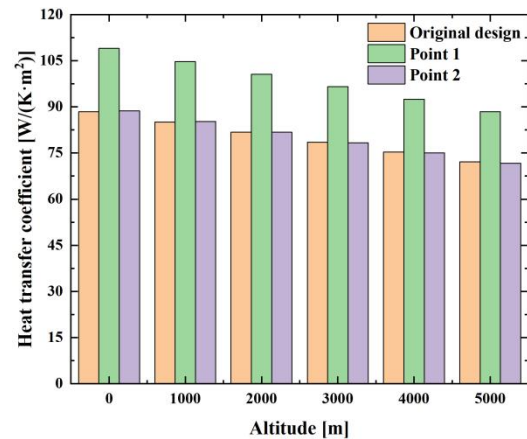
However, this configuration also leads to less enhancement in heat transfer. Conversely, solutions in the high heat transfer coefficient region exhibit higher pressure drops compared to the original design, reflecting a design trade-off where increased flow resistance might be accepted in order to improve thermal efficiency. Fins in this region typically feature smaller spacings and greater lengths. The reduced spacing enhances turbulence and promotes heat exchange, while the extended fin length increases the heat transfer area. These combined effects significantly improve the heat transfer coefficient, albeit at the cost of elevated flow resistance. The comprehensive optimization region demonstrates improvement in both objectives, with lower pressure drop and higher heat transfer coefficient relative to the baseline design. Fins in this region are characterized by moderate fin length and relatively large spacing; this configuration maintains sufficient heat transfer area while avoiding excessive flow disturbance. The appropriately larger spacing reduces flow resistance, which together with the moderate fin length, yields adequate turbulence; therefore, an optimal balance between pressure drop and heat transfer performance is achieved.

To further validate the optimization results, two extreme representative points were selected from the

Pareto solutions in the comprehensive optimization region: these were the design with the lowest pressure drop, and the design with the highest heat transfer coefficient. Their structural parameters were substituted into *Fluent* software for numerical simulations; their performance was compared with that of the original design under five different altitude conditions. The comparative results are shown in Fig. 15. The findings demonstrate that across all tested altitude conditions, when the pressure drop is comparable to that of the original structure, the heat transfer coefficient increases by approximately 23%; conversely, when the heat transfer coefficient is similar to that in the original design, the pressure drop is reduced by about 17%. To provide a more intuitive and precise comparison, the detailed performance data and the specific percentage improvements for the optimized designs (Point 1 and Point 2) relative to the original design across varying altitudes are summarized in Table S4 in the ESM. These results confirm the effectiveness and practical engineering value of the proposed optimization method.



(a) Comparison of pressure drops



(b) Comparison of heat transfer coefficients

Fig. 15 Comparison of the results before and after optimization

## 4 Conclusions

In this study we systematically investigated the variation of the thermohydraulic performance of staggered fin heat exchangers with altitude, focusing on an altitude range of 0-5000 meters. On this basis, a set of optimization methods for such fin structures was established by integrating machine learning (ML) and multi-objective optimization algorithms. The results demonstrate that high altitude conditions significantly degrade fin performance, but the proposed ML-aided optimization framework can effectively mitigate this issue.

First off, the increase in altitude significantly reduces air density and pressure, leading to a noticeable decline in the flow and heat transfer performance of staggered fins. At an altitude of 5000 meters, the pressure drop and heat transfer coefficient decreased by 23% and 18%, respectively, compared to sea level; boundary layer thickening was identified as the physical mechanism governing this performance degradation.

Moreover, microscopic analysis indicated that under high-altitude conditions, the near-wall temperature and velocity gradients weaken, with the thermal and velocity boundary layer thicknesses increasing by 24% and 19%, respectively. These effects led to a significant reduction in the effective heat transfer area.

Among the three ML models evaluated, the GBDT demonstrated the best predictive performance

(with  $R^2$  approaching 1.0 and a minimal  $RMSE$ ), making it suitable for high-precision prediction and multi-objective optimization of fin heat dissipation performance.

Finally, multi-objective optimization based on the GBDT model and an improved NSGA-II algorithm successfully achieved targeted improvements in the staggered fin structure. For the optimized fins in the comprehensive performance region, validation across different altitudes demonstrated remarkable augmentations: when their pressure drop was comparable to that of the original fin structure, the heat transfer coefficient increased by about 23% under all tested altitude scenarios; conversely, when their heat transfer coefficient remained on par with the original design, the pressure drop decreased by about 17% across various altitudes. This optimized solution therefore shows promise for heat exchanger design in high-altitude environments.

### Acknowledgments

This work is supported by the Youth Science Fund Project of the National Natural Science Foundation of China (No. 52206027).

### Author contributions

Kai Zhao: conceptualization, validation, investigation, and writing—original draft preparation. Chunming Shao: conceptualization, formal analysis, and project administration. Xiaoxia Sun: methodology, formal analysis, writing—original draft preparation, supervision, and funding acquisition. Yuanqing Xia: methodology, resources, supervision, and funding acquisition. Qiangqiang Li: software, investigation, and visualization. Lili Shen: software, data curation, and visualization. Min Lin: validation and data curation. Zhi Li: validation and resources.

### Conflict of interest

Kai Zhao, Chunming Shao, Xiaoxia Sun, Yuanqing Xia, Qiangqiang Li, Lili Shen, Min Lin, and Zhi Li declare that they have no conflict of interest.

### Declaration on the use of generative AI tools

The authors declare that they did not use any generative artificial intelligence tools in the preparation or writing of this manuscript.

### Data availability

The data that support the findings of this study are available from the corresponding author upon reasonable request.

### References

- Ben-Nakhi A, Chamkha AJ, 2006. Effect of length and inclination of a thin fin on natural convection in a square enclosure. *Numerical Heat Transfer, Part A: Applications*, 50(4):381-399. <https://doi.org/10.1080/10407780600619907>
- Cai Huikun, Zhang Yinliang, Liao Yidai, et al., 2017. Performance Analysis of Different Radiator Fins at Various Altitudes. *Journal of South China University of Technology. Natural Science Edition*, 45(2):91 - 98.
- Chen GS, Sun M, Li JD, et al., 2024. Study on high-altitude ceiling strategy of compression ignition aviation piston engines based on BP-NSGA II algorithm optimization. *Energy*, 294:130966. <https://doi.org/10.1016/j.energy.2024.130966>
- Elsayed ML, Mesalhy O, Kizito JP, et al., 2020. Performance of a guided plate heat sink at high altitude. *International Journal of Heat and Mass Transfer*, 147:118926. <https://doi.org/10.1016/j.ijheatmasstransfer.2019.118926>
- He ZX, Yu QH, Ye JD, et al., 2024. Optimization of plate-fin heat exchanger performance for heat dissipation of thermoelectric cooler. *Case Studies in Thermal Engineering*, 53:108668. <https://doi.org/10.1016/j.csite.2023.103953>
- Huang Q, Xie TF, Liu JL, 2025. Machine Learning-Assisted Reconstruction of In-Cylinder Pressure in Internal Combustion Engines Under Unmeasured Operating Conditions. *Energies*, 18(19):5235. <https://doi.org/10.3390/en18195235>
- Miao L, Wan R, Qiao K, et al., 2025. Fluid flow and heat transfer characteristics of flying-wing finned tubes in high-altitude environments. *International Journal of Thermal Sciences*, 217: 110059. <https://doi.org/10.1016/j.ijthermalsci.2025.110059>
- Mustafa NE, Kandlikar SG, 2025. Performance Evaluation of Boiling Chamber With Microchannel Chip and Taper Microgap. *ASME Journal of Heat and Mass Transfer*, 147(12):121604. <https://doi.org/10.1115/1.4069269>
- Kays.W.M, London.A.L, 1984. *Compact Heat Exchangers*, third ed., McGraw-Hill, New York.
- Lang L, Liu ZJ, Liu YS, et al., 2024. Performance analysis of a compact offset strip fin heat exchanger for lubrication system in aero engine. *Journal of Thermal Science and Engineering Applications*, 16(7):071006. <https://doi.org/10.1115/1.4065357>
- Li JH, Su JT, Wang SX, 2025. Research on the Performance of Radiators in Hybrid Vehicle Thermal Management Systems. *World Electric Vehicle Journal*, 16(2):89. <https://doi.org/10.3390/wevj16020089>
- Li K, Wen J, Wang SM, et al., 2020. Multi-parameter optimization of serrated fins in plate-fin heat exchanger based on fluid-structure interaction. *Applied Thermal Engineering*, 176:115357. <https://doi.org/10.1016/j.applthermaleng.2020.115357>
- Li YW, Wang YC, Wan R, et al., 2022. Study on the air-side

- flow and heat transfer characteristics of corrugated fin under low-pressure environment. *Experimental Heat Transfer*, 35(1):62 - 78. <https://doi.org/10.1080/08916152.2020.1818886>
- Liu ZT, Liu JL, 2022. Effect of altitude conditions on combustion and performance of a turbocharged direct-injection diesel engine. *Proceedings of the Institution of Mechanical Engineers Part D-Journal of Automobile Engineering*, 236(4):582 - 593. <https://doi.org/10.1177/09544070211026204>
- Liu ZT, Sun MY, Huang YQ, et al., 2020. Investigation of heat transfer characteristics of high-altitude intercooler for piston aero-engine based on multi-scale coupling method. *International Journal of Heat and Mass Transfer*, 156:119898. <https://doi.org/10.1016/j.ijheatmasstransfer.2020.119898>
- Ramakrishnan KR, Ahmed S, Ekkad S, et al., 2022. Characterization of transient wall heat load for a low NOx lean premixed swirl stabilized can combustor under reacting conditions. *Journal of Thermal Science and Engineering Applications*, 14(2):021012. <https://doi.org/10.1115/1.4051375>
- Sadeghi HM, Babayan M, Chamkha AJ, 2020. Investigation of using multi-layer PCMs in the tubular heat exchanger with periodic heat transfer boundary condition. *International Journal of Heat and Mass Transfer*, 147:118970. <https://doi.org/10.1016/j.ijheatmasstransfer.2019.118970>
- Shahsavari A, Goodarzi A, Askari IB, et al., 2022. The entropy generation analysis of the influence of using fins with tip clearance on the thermal management of the batteries with phase change material: Application a new gradient-based ensemble machine learning approach. *Engineering Analysis with Boundary Elements*, 140:432 - 446. <https://doi.org/10.1016/j.enganabound.2022.04.024>
- Sun QP, Li XL, Liu XL, et al., 2024. A coordinated mode switch control strategy for a two-gear power-split hybrid system. *Machines*, 12(7):427. <https://doi.org/10.3390/machines12070427>
- Tikadar A, Kumar S, 2024. Machine learning approach to predict heat transfer and fluid flow characteristics of integrated pin fin-metal foam heat sink. *Numerical Heat Transfer Part B-Fundamentals*, 85(11):1533 - 1558. <https://doi.org/10.1080/10407790.2023.2266772>
- Wen ZX, Wu JL, Cao XW, et al., 2024. Machine learning and prediction study on heat transfer of supercritical CO<sub>2</sub> in pseudo-critical zone. *Applied Thermal Engineering*, 243:122630. <https://doi.org/10.1016/j.applthermaleng.2024.122630>
- Xie YH, Wang XF, 2025. Prediction of Thermal and Optical Properties of Oxyfluoride Glasses Based on Interpretable Machine Learning. *Nanomaterials*, 15(11):860. <https://doi.org/10.3390/nano15110860>
- Xu ZD, Han YG, Ren DF, et al., 2022. An approach of multistage connected ventilation cooling structure for armored vehicle thermal management. *Journal of Thermal Science and Engineering Applications*, 14(2):021008. <https://doi.org/10.1115/1.4051370>
- Yang CH, Liu RL, Jiao YF, et al., 2024. Study on thermodynamic matching optimization of variable flow cooling system of diesel engine at high altitudes. *Energy Sources, Part A: Recovery, Utilization, and Environmental Effects*, 46(1):8787 - 8805. <https://doi.org/10.1080/15567036.2020.1769777>
- Yang RM, Liu JH, Liu ZT, et al., 2024. Applying separate treatment of fuel- and air-borne nitrogen to enhance understanding of in-cylinder nitrogen-based pollutants formation and evolution in ammonia-diesel dual fuel engines. *Sustainable Energy Technologies and Assessments*, 69:103910. <https://doi.org/10.1016/j.seta.2024.103910>
- Zhao JL, Yang RM, Ye PY, et al., 2026. SHAP-BASED INTERPRETABLE ENSEMBLE LEARNING FOR PREDICTING HEAT TRANSFER PERFORMANCE IN MICROCHANNEL HEAT EXCHANGERS WITH LOUVERED FINS. *Heat Transfer Research*, 57(2):67 - 93. <https://doi.org/10.1615/HeatTransRes.2025058567>

### Electronic supplementary materials

Section S1-S5, Table S1-S4, Figs. S1-S4